Dynamic and accurate assessment of acetaminophen-induced hepatotoxicity by integrated photoacoustic imaging and mechanistic biomarkers in vivo

Brillant, Nathalie ; Elmasry, Mohamed ; Burton, Neal C ; Rodriguez, Josep Monne ; Sharkey, Jack W ; Fenwick, Stephen ; Poptani, Harish ; Kitteringham, Neil R ; Goldring, Christopher E ; Kipar, Anja ; Kevin Park, B ; Antoine, Daniel J

Abstract: The prediction and understanding of acetaminophen (APAP)-induced liver injury (APAP-ILI) and the response to therapeutic interventions is complex. This is due in part to sensitivity and specificity limitations of currently used assessment techniques. Here we sought to determine the utility of integrating translational non-invasive photoacoustic imaging of liver function with mechanistic circulating biomarkers of hepatotoxicity with histological assessment to facilitate the more accurate and precise characterization of APAP-ILI and the efficacy of therapeutic intervention. Perturbation of liver function and cellular viability was assessed in C57BL/6J male mice by Indocyanine green (ICG) clearance (Multispectral Optoacoustic Tomography (MSOT)) and by measurement of mechanistic (miR-122, HMGB1) and established (ALT, bilirubin) circulating biomarkers in response to the acetaminophen and its treatment with acetylcysteine (NAC) in vivo. We utilised a 60% partial hepatectomy model as a situation of defined hepatic functional mass loss to compared acetaminophen-induced changes to. Integration of these mechanistic markers correlated with histological features of APAP hepatotoxicity in a time-dependent manner. They accurately reflected the onset and recovery from hepatotoxicity compared to traditional biomarkers and also reported the efficacy of NAC with high sensitivity. ICG clearance kinetics correlated with histological scores for acute liver damage for APAP (i.e. 3h timepoint; $r=0.90$, $P<0.0001$) and elevations in both of the mechanistic biomarkers, miR-122 (e.g. 6h timepoint; $r=0.70$, $P=0.005$) and HMGB1 (e.g. 6h timepoint; $r=0.56$, $P=0.04$). For the first time we report the utility of this non-invasive longitudinal imaging approach to provide direct visualisation of the liver function coupled with mechanistic biomarkers, in the same animal, allowing the investigation of the toxicological and pharmacological aspects of APAP-ILI and hepatic regeneration.

DOI: https://doi.org/10.1016/j.taap.2017.07.019

Brillant, Nathalie; Elmasry, Mohamed; Burton, Neal C; Rodriguez, Josep Monne; Sharkey, Jack W; Fenwick, Stephen; Poptani, Harish; Kitteringham, Neil R; Goldring, Christopher E; Kipar, Anja; Kevin Park, B; Antoine, Daniel J (2017). Dynamic and accurate assessment of acetaminophen-induced hepatotoxicity by integrated photoacoustic imaging and mechanistic biomarkers in vivo. Toxicology and applied pharmacology, 332:64-74.
DOI: https://doi.org/10.1016/j.taap.2017.07.019

Accepted Manuscript

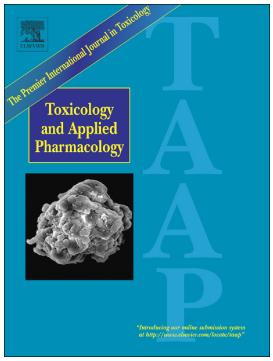

Dynamic and accurate assessment of acetaminophen-induced hepatotoxicity by integrated photoacoustic imaging and mechanistic biomarkers in vivo

Nathalie Brillant, Mohamed Elmasry, Neal C. Burton, Josep M. Monne, Jack W. Sharkey, Stephen Fenwick, Harish Poptani, Neil R. Kitteringham, Christopher E. Goldring, Anja Kipar, B. Kevin Park, Daniel J. Antoine

PII: S0041-008X(17)30316-2
DOI: doi: 10.1016/j.taap.2017.07.019
Reference: YTAAP 14016

To appear in: *Toxicology and Applied Pharmacology*

Received date: 8 June 2017
Revised date: 22 July 2017
Accepted date: 25 July 2017

Please cite this article as: Nathalie Brillant, Mohamed Elmasry, Neal C. Burton, Josep M. Monne, Jack W. Sharkey, Stephen Fenwick, Harish Poptani, Neil R. Kitteringham, Christopher E. Goldring, Anja Kipar, B. Kevin Park, Daniel J. Antoine , Dynamic and accurate assessment of acetaminophen-induced hepatotoxicity by integrated photoacoustic imaging and mechanistic biomarkers in vivo. The address for the corresponding author was captured as affiliation for all authors. Please check if appropriate. Ytaap(2017), doi: 10.1016/j.taap.2017.07.019

Dynamic and accurate assessment of acetaminophen-induced hepatotoxicity by integrated photoacoustic imaging and mechanistic biomarkers in vivo

Nathalie Brillant[*], Mohamed Elmasry[*], Neal C. Burton [†], Josep M. Monne[‡], Jack W Sharkey[§], Stephen Fenwick[¶], Harish Poptani[§], Neil R. Kitteringham[*], Christopher E. Goldring[*], Anja Kipar [‖, ǁǁǁ], B. Kevin Park[*] and Daniel J. Antoine[*]

[*]Department of Molecular & Clinical Pharmacology, MRC Centre for Drug Safety Science, Institute of Translational Medicine, University of Liverpool, Liverpool, UK.

[†]iThera Medical, Munich, Germany.

[‡]Department of Veterinary Pathology, Institute of Veterinary Science, University of Liverpool, Liverpool, UK.

[§]Department of Cellular & Molecular Physiology, Institute of Translational Medicine, University of Liverpool, Liverpool, UK.

[¶]General Surgery, Aintree University Hospital, Liverpool, Merseyside, UK.

[‖]Institute of Global Health, University of Liverpool, Liverpool, UK

[ǁǁǁ]Institute of Veterinary Pathology, Vetsuisse Faculty, University of Zurich, Zurich, Switzerland.

Conflict of Interest

The authors have no conflict of interest to report

Author contributions

NB and DJA wrote the article; NB, NCB, BKP and DJA designed the research; NB, ME, JWS and HP performed research; NB, NCB, JM, HP and AK analysed data; SF, NK and CEG provided resources and intellectual support; all authors contributed to the final article.

Author for correspondence

Daniel J Antoine, PhD

d.antoine@liverpool.ac.uk, +44 151 795 5460

ABSTRACT

The prediction and understanding of acetaminophen (APAP)-induced liver injury (APAP-ILI) and the response to therapeutic interventions is complex. This is due in part to sensitivity and specificity limitations of currently used assessment techniques. Here we sought to determine the utility of integrating translational non-invasive photoacoustic imaging of liver function with mechanistic circulating biomarkers of hepatotoxicity with histological assessment to facilitate the more accurate and precise characterization of APAP-ILI and the efficacy of therapeutic intervention.

Perturbation of liver function and cellular viability was assessed in C57BL/6J male mice by Indocyanine green (ICG) clearance (Multispectral Optoacoustic Tomography (MSOT)) and by measurement of mechanistic (miR-122, HMGB1) and established (ALT, bilirubin) circulating biomarkers in response to the acetaminophen and its treatment with acetylcysteine (NAC) in vivo. We utilized a 60% partial hepatectomy model as a situation of defined hepatic functional mass loss to compared acetaminophen-induced changes to.

Integration of these mechanistic markers correlated with histological features of APAP hepatotoxicity in a time-dependent manner. They accurately reflected the onset and recovery from hepatotoxicity compared to traditional biomarkers and also reported the efficacy of NAC with high sensitivity. ICG clearance kinetics correlated with histological scores for acute liver damage for APAP (i.e 3h timepoint; $r = 0.90$, $P < 0.0001$) and elevations in both of the mechanistic biomarkers, miR-122 (e.g. 6h timepoint; $r = 0.70$, $P = 0.005$) and HMGB1 (e.g. 6h timepoint; $r = 0.56$, $P = 0.04$).

For the first time we report the utility of this non-invasive longitudinal imaging approach to provide direct visualisation of the liver function coupled with mechanistic

biomarkers, in the same animal, allowing the investigation of the toxicological and pharmacological aspects of APAP-ILI and hepatic regeneration.

Key words

Acetaminophen; biomarker; Drug-Induced Liver Injury; HMGB1; miR-122; MSOT

Abbreviations

ALI; acute liver injury, ALF; acute liver failure, microRNA-122; miR-122, High Mobility Group Box 1; HMGB1), TBIL; total bilirubin, ICG; indocyanine green, MSOT; multispectral optoacoustic tomography, PH; partial hepatectomy, APAP; Acetaminophen, NAC; N-Acetyl-cysteine, Alanine Aminotransferase (ALT), MRI; Magnetic resonance imaging, GSH; glutathione

INTRODUCTION

Drug-induced liver injury (DILI) is a frequent cause for safety concern in preclinical and clinical drug development. It is also a leading cause of post-market withdrawal leading to regulatory action. Acute liver failure (ALF) is a feared complication of DILI, carrying a high risk of morbidity and mortality (Reuben *et al.*, 2016). A lack of sensitivity, specificity and an indirect mechanistic basis of currently used circulating biomarkers and assessment methods of hepatic injury has been widely cited as a significant factor for limited predictivity and understanding of DILI (Clarke *et al.*, 2016; Antoine and Dear, 2017). Development of an experimental "toolbox" that encompasses the measurement of mechanistic events and changes in liver function alongside the viability and activity of both parenchymal and non-parenchymal cells in a non-invasive, time dependent and longitudinal way could prove essential for the detection, aetiological diagnosis, and prediction and monitoring of potential therapeutic interventions for DILI. Additionally, the validation of the non-invasive imaging assessment of liver function that can be repeated in individual animals would overcome limitations in preclinical studies such as small blood volumes and obtaining liver tissue following sacrifice.

Clinical and preclinical studies of DILI have identified and developed circulating biomarkers that provide enhanced hepatic specificity (microRNA-122; miR-122) and provide information on mechanistic events such as hepatocyte necrosis (keratin-18), apoptosis (caspase-cleaved keratin-18), mitochondrial dysfunction (glutamate dehydrogenase), induction of inflammation (acetyl-High Mobility Group Box 1; acetyl-HMGB1) and regeneration (Colony Stimulating Factor 1; CSF-1) (Wang *et al.*, 2009; Starkey Lewis *et al.*, 2011; Antoine *et al.*, 2012; McGill *et al.*, 2012; Stutchfield *et al.*, 2015). Moreover, specific subsets of these mechanistic markers have also been

demonstrated to allow early identification of liver injury (miR-122) and can support enhanced prognostic determination in man (acetyl-HMGB1, CSF-1) (Antoine *et al.*, 2012; Antoine *et al.*, 2013; Stutchfield *et al.*, 2015). Although these key attributes have been recognised as fundamental to efforts in translational hepatotoxicity research and have gain support by drug regulators (EMA, 2016; FDA, 2016), many of the reported candidate biomarkers for hepatic drug safety have focused on hepatocyte injury rather than liver function. Despite its highly specialized function, the liver is unique in its capacity to adapt to chemical insults (Aleksunes *et al.*, 2008; Eakins *et al.*, 2015) and to regenerate after massive liver resection (Riehle *et al.*, 2011). The ability of the liver to functionally cope with metabolic needs in different life threatening scenarios open a door to novel assessments directed towards the analysis and quantification of the remaining functional liver mass rather than the irreversible hepatic dead mass.

The elimination of the water-soluble, hydrophobic organic anion, FDA approved dye Indocyanine green (ICG) is dependent upon its non-ATP-dependent transport by organic anion transporting polypeptides (OATPs) and sodium-taurocholate co-transporting polypeptide (NTCPs) (de Graaf *et al.*, 2011) into the hepatic parenchyma and excretion into the bile through ATP-dependent transporters multidrug resistance P-glycoprotein (Mdr2) and multidrug resistance-associated protein (Mrp2) (Wheeler *et al.*, 1958; Huang and Vore, 2001). This dye mainly binds to plasma proteins (albumin and α1-lipoproteins) after intravenous administration without any extravascular distribution and without entering into the enterohepatic circulation is mainly taken by the hepatocytes and without any metabolic change is excreted into the gallbladder (Sakka *et al.*, 2002; Olmedilla *et al.*, 2009). Due to its exclusive hepatic clearance, the ICG elimination rate has been widely used to assess hepatic

blood flow, hepatosplanchnic haemodynamics, and liver function (Imamura *et al.*, 2005; Sakka, 2007; Levesque *et al.*, 2016).

The non-invasive and dynamic assessment of ICG clearance *in vivo* has recently been made possible through the development of multispectral optoacoustic tomography (MSOT). This novel non-invasive imaging modality exhibits improved resolution and optical imaging sensitivity combined with excellent temporal resolution and deep tissue penetration depth (Wang *et al.*, 2003; Zhang *et al.*, 2006). Recent applications have revealed its utility for *in vivo* imaging in oncology (McNally *et al.*, 2016), human vasculature (Taruttis *et al.*, 2016), neurology (Dima *et al.*, 2014) and nephrotoxicity (Scarfe *et al.*, 2015) applications as well as in the clinic for the non-invasive imaging of Crohn's disease and assessment of the metastatic status in melanoma (Stoffels *et al.*, 2015; Waldner *et al.*, 2016).

Therefore, the purpose of this investigation was to establish for the first time an experimental "tool box" that uses a novel non-invasive, dynamic imaging modality to assess hepatic function, providing additional insights beyond the classical serum markers of liver damage and allowing the preclinical stratification for entry into studies for assessing utility of therapeutic interventions. Using APAP as a model hepatotoxin, the aim of these studies is to integrate this approach with mechanistic circulating biomarkers of hepatotoxicity, that have enhanced sensitivity and specificity, alongside traditional histopathological evaluation to potentially enhance the understanding and prediction of the onset and recovery from DILI and the response to therapeutic interventions.

MATERIALS AND METHODS

Animal treatment

All animals received humane care and the protocols described were in accordance with criteria outlined in a license granted under the Animals (Scientific Procedures) Act 1986 and approved by the University of Liverpool Animal Ethics Committee. Acetaminophen (APAP) was chosen as a hepatotoxin model and male C57BL/6J mice (Charles River, Margate, UK), aged seven to eight weeks were used. These were group housed (n = 5) with free access to food and water with a seven-day acclimatization period. Animals were fasted for 14 h prior to APAP dosing. For the time course study, groups of randomly selected animals were administered 300 mg/kg of APAP (Sigma Aldrich, UK) in 0.9 % saline (Braun, Melsungen, Germany) or 0.9 % saline (control) with a single intraperitoneal (i.p.) injection. Mice were imaged at 3 h (control, n = 10; APAP, n = 10), 6 h (control, n = 5; APAP, n = 10), 24 h (control, n = 5, APAP, n = 10), 48 h (control, n = 4; APAP, n = 6), 72 h (control, n = 4 euthanised; APAP, n = 6) and 96 h (control, n = 5; APAP, n = 5) post APAP dosing and euthanized immediately after imaging.. Timepoints were selected according to the insignificant changes in circulating biomarkers seen in previous studies before 3 h (Antoine *et al.*, 2009) and the full recovery seen at 96 h in the histological examination, the gold standard technique to diagnose liver disease (Tannapfel *et al.*, 2012).

In order to preclinically test the utility of MSOT imaging to monitor liver function non-invasively and repeatedly in a small cohort, another group of mice (n = 5) was imaged throughout the same timeline after APAP administration and animals were only euthanized at the end of the course (96 h).

Additionally, to examine the capacity of MSOT to report the efficacy of established therapeutics, a cohort of mice was treated with 500 mg/kg of acetylcysteine (NAC) in phosphate-buffered saline (PBS) pH = 7, 1 h after APAP dose, imaged at 6 h (n = 10) and 24 h (n = 10) post APAP dosing and euthanised immediately after.

Partial Hepatectomy surgery procedure

Partial hepatectomy (PH) was used as a known volume of functional hepatic mass loss to compare with the effect of APAP and its amelioration with NAC. Mice (n = 5 per group) were group housed (n= 5) with free access to food and water with a seven-day acclimatisation period. Mice underwent surgery under sterile conditions. A midline laparotomy incision was drawn to expose the xiphoid process. The falciform ligament was divided and the median and left lateral liver lobes externalised. Lobes were ligated at the base of each lobe using 4/0 silk ties and removed. The peritoneum and the skin were closed using 6-0 Vicryl™ sutures. Mice received subcutaneous injections of Buprenorphine (0.05 mg/kg) as analgesia. Sham operation was performed in a cohort of mice (n = 5) as a control group where animals underwent the same procedure as the PH mice, without removing the liver lobes. These animals were then imaged to assess liver volume by means of magnetic resonance imaging (MRI) and liver function by means of MSOT imaging at day 1, 2, 3 and 7 after surgery. Liver volume was assessed by MRI until day 10 after surgery where full recovery of hepatic volume was observed (data not shown).

Circulating biomarker measurements and histological examination

Animals were euthanised by rising CO_2 inhalation and blood was collected by cardiac puncture. Blood samples were stored at 4°C and allowed to clot for 30 min, then

separated into serum (2,000 x g, 10 min, 4 °C). ALT, miR-122 and total HMGB1 were measured as previously described (Antoine *et al.*, 2009; Antoine *et al.*, 2010; Starkey Lewis *et al.*, 2011; Antoine *et al.*, 2012; Antoine *et al.*, 2013). Serum ALT activity was determined by kinetic assay according to the manufacturer's instructions (Thermo Fisher) and assayed on a Varioskan Flash machine (Thermo Fisher). MiR-122 was extracted and purified using a miRNeasy kit followed by an RNeasy MiniElute Cleanup Kit (Qiagen, Venlo, Netherlands), in accordance with the manufacturer's instructions. Reverse transcription was performed using the TaqMan miRNA reverse transcription kit (Applied Biosystems) and miR-22 (and U6 as an endogenous control according to previous published data) primers using a GeneAmp PCR9700 machine and qPCR reactions were run using Taqman PCR primers and Master mix (Applied Biosystems) on a ViiA7 machine (Life Technologies). Total HMGB1 measurement was determined by sandwich ELISA according to the manufacturer's instructions (Shino-Test/IBL international) and total bilirubin (TBIL) was measured using a Bilirubin Assay Kit (Sigma-Aldrich) following the manufacturer's instructions. Livers were removed, and the left lateral lobe fixed in 10% neutral buffered formalin for approximately 48 h and routinely paraffin wax embedded. Consecutive sections (3-5 μm) were prepared and routinely stained with haematoxylin-eosin (HE) and subjected to the Periodic Acid Schiff (PAS) reaction for the demonstration of glycogen within hepatocytes, respectively. They were histologically assessed for any pathological changes and the APAP-induced hepatotoxic changes scored blindly as previously described and summarized in supplementary figure 1 (Antoine *et al.*, 2009; Antoine *et al.*, 2010). The score for hepatocyte necrosis (drug-induced liver injury score; DILI score) for each animal was based on the average of all lobules in the liver section (0: no necrosis; 1: necrosis

present, but ≤ 25 % of the lobules affected; 2: > 25 ≤ 50% of the lobules affected; 3: > 50 of the lobules affected; 4: ≤ 75% of the lobules affected; 5: > 75% of the lobules affected). This scoring was then used to correlate the degree of liver injury and ICG half-life in the mice at 6 h, 24 h, 48 h, 72 h and 96 h post dosing. In the mice examined at 3 h post APAP dosing, a score was established reflecting the extent of centrilobular hydropic degeneration (HD) (score for degenerative changes) based on the number of the innermost centrilobular hepatocyte layers that were affected (1: 1-2 layers with HD; 2: 2-3 layers with HD; 3: 3-4 layers with HD; 3.5: 3-5 layers with HD; 4: 4-5 layers with HD), again, an average score was determined for each mouse.

Determination of total hepatic Glutathione (GSH)

Total GSH content was quantified by the 5-5'-Dithiobis (2-nitrobenzoic acid) (DTNB)-based 'recycling' method as previously described (Owens and Belcher, 1965). Hepatic GSH was measured by homogenizing weighed mouse liver samples (30-50 mg) in 800 µl of a buffered solution containing 6.3 mM EDTA and 143 mM NaH_2PO_4, pH 7.4 and 200 µl of 6.5 % (w/v) SSA. The solution was centrifuged at 14,000 rpm for 5 min. The pellets were dissolved in 1 M NaOH at 60 °C for 1 h and reserved for protein concentration determination by the method of Bradford using Bio-Rad protein assay at 570 nm (Bradford, 1976). The supernatants were used to measure GSH concentration spectromically (at 412 nm) by kinetic reaction between total GSH and glutathione reductase on a MRX microtiter-plate reader with Max Revelation software (Dynatech Laboratories, Billinghirst, UK) as described previously (Williams *et al.*, 2007). GSH was compared to a 0-40 nmol/ml standard curve.

ICG clearance measurement by means of multispectral optoacoustic tomography (MSOT)

For optoacoustic imaging, an MSOT inVision 256-TF small animal imaging system (iThera Medical GmbH, Munich, Germany) was used (Morscher *et al.*, 2014). Briefly, a tunable optical parametric oscillator (OPO) pumped by an Nd:YAG laser provides excitation pulses with a duration of 9 ns at wavelengths from 680 nm to 980 nm at a repetition rate of 10 Hz with a wavelength tuning speed of 10 ms and a peak pulse energy of 100 mJ at 730 nm. Ten arms of a fiber bundle provide even illumination of a ring-shaped light strip of approximately 8 mm width. For ultrasound detection, 256 toroidally focused ultrasound transducers with a center frequency of 5 MHz (60 % bandwidth), organized in a concave array of 270 degree angular coverage and a radius of curvature of 4 cm, were used.

ICG (Pulsion Medical Systems, Germany) stock (5 mg/ml in sterile dH_2O) was diluted in 0.9 % saline to 40 nmol in a final volume of 200ul for blood vessel imaging. At 3, 6, 24, 48, 72 and 96 h after APAP or saline administration, mice were anaesthetised (isoflurane) and had hair removed by shaving and depilatory cream from the abdominal and lumbar region. They were then imaged in the inVision 256-TF MSOT imaging system. This was performed using a multispectral protocol for 23 min. The acquisition rate was 10 frames per second using wavelengths 700, 730, 760, 800, 850 and 900 nm. Ten consecutive frames were averaged to minimise motion-induced perturbations in the image quality. After 3 min of baseline imaging, the mice received 220 µl (40 nmol) ICG fluorescent dye in 0.9 % saline through a tail vein cannula over a period of 10 s. Following this the imaging data was continuously acquired for another 20 min. Data was reconstructed using ViewMSOT^{TM} using a

back projection algorithm with impulse response and multispectral processing performed using linear regression with ICG, and oxy- and deoxy-hemoglobin spectra to resolve signals for the ICG dye, including gradient scaling for each animal at a time prior to the injection of the ICG. Regions of interest (ROIs) drawn around the ischiatic vessels of each mouse were used to determine the mean peak pixel intensity value (MSOT arbitrary units). The MSOT signal over time for mean ischiatic vessel pixel intensities was fitted in the PK GUI_v6_04 MSOT software program to an exponential decay model to determine the characteristic excretion half-life and rate constant.

Statistical analyses

Pearson and Spearman correlation coefficients models were applied to test whether the type and extent of the histological changes and the serum biomarker fluctuations were correlated with ICG measurements. Standard error of the mean was measured for all the different groups and parameters. Independent t-tests and one way ANOVA test were used when applied to compare measures of liver impairment, serum biomarker changes and quantitative histological scores at different time points between the control and the treatment group. The assumption of normality of variance was previously assessed and *post hoc* test was applied accordingly (Tukey).

RESULTS

Characterisation of the time course of acetaminophen hepatotoxicity by novel and established circulating biomarkers and histopathology

To induce DILI we utilised our previously reported and well-established murine model of APAP-hepatotoxicity (Lundback *et al.*, 2016). To assess the time course of liver injury, we measured serum ALT activity and total bilirubin (TBIL) as well as liver-enriched miR-122 and total high-mobility group box-1 protein (HMGB1) in sera and performed a histopathological evaluation of the livers. Significant elevations in ALT (1055.8±208.6 U/I), TBIL (0.74±0.04 mg/dL), miR-122 (10028.1 ±5151.6 U6 normalised) and HMGB1 (141.5±27.6 ng/ml) were evident as early as 3 h after APAP dosing (**Figure 1A-D**); at this point, evidence of centrilobular hepatocyte death was restricted to apoptosis of rare individual hepatocytes. However, there was evidence of complete hepatocellular loss of glycogen in the parenchyma (Figure 1E). The innermost centrilobular hepatocyte layers (up to 5 layers) exhibited hydropic degeneration, a feature consistent with cell damage **(Figure 1E)**. By 6 h post dosing, when the histological examination revealed substantial hepatocyte death (coagulative necrosis; median score 2; **Figure 1E**), miR-122 levels and serum ALT activity had increased further, whereas TBIL and HMGB1 levels had already dropped substantially. Both showed a further decrease at 24 h post dosing, when miR-122 levels had also dropped and only ALT exhibited peak values (3401.7±607.9 U/l). At this point, the histological picture was similar to that at 6 h (median score 2.25), though there was in general evidence of glycogen restitution outside affected areas **(Figure 1E).** By 48 h, necrotic hepatocytes were less numerous (median score 1) and intermingled with small (new) hepatocytes, there was also mild to moderate neutrophil-dominated leukocyte infiltration stretching from central veins into the

adjacent sinuses. Outside affected areas, the parenchyma exhibited full glycogen restitution **(Figure 1E)**. At 72 and 96 h, necrotic cells were not observed anymore, centrilobular areas were increasingly cell rich, and several mitotic hepatocytes were observed, all consistent with resolution of liver damage by regeneration. Also, there was a variable amount of infiltrating leukocytes in particular at 96 h **(Figure 1E)**. A decreasing trend in all biomarkers was observed over the time course assessed, with miR-122 and HMGB1 concentrations returning to baseline values by 72 and 96 h. However, although ALT and TBIL had decreased by 96 h, these values were still statistically significantly higher than those of control mice **(Figure 1A-D)**.

ICG clearance is impaired *in vivo* during APAP-ILI

To investigate the potential of non-invasive imaging to evaluate liver function during APAP-induced liver injury, ICG clearance was monitored in real-time between 3 and 96 h post-APAP challenge from the ischiatic vessels, by MSOT **(Figure 2A-F)**. Compared to vehicle control mice ($t_{1/2}$= 36.2 s) (Figure A, C), the elimination of ICG through the liver of APAP-injured mice was statistically significantly impaired (i.e. 6h timepoint; $t_{1/2}$=155.2 s) (Figure 2 B, D). The increase in ICG half-life also demonstrated time-dependence, showing a biphasic response with the most elevated change observed at 3 h (152.0 ±25.1s), a gradual return to baseline levels by 24 h with the second peak observed at 48 h post-APAP treatment **(Figure 2E)**. This trend was also seen when ICG clearance was expressed as a function of its rate constant (3 h data, 0.004±0.0005 s compared to time matched controls 0.02 ±0.001 s) **(Figure 2F)**. By 96 h, ICG-measured clearance was not different to time-matched saline-treated controls **(Figure 2E-F)**.

To establish a reference model of defined hepatic functional mass and subsequent regeneration that correlates with ICG clearance, mice were subjected to a 60% hepatectomy. MRI was used to define the actual degree of hepatic mass loss following hepatectomy and hepatic regrowth over 7 days (Figure 3 A-D). Active liver regeneration was observed from day 2 after surgery onwards, with full recovery in hepatic mass by day 10 (data not shown). As a result of 60 % hepatectomy, mice showed significantly decreased hepatic function with a peak in MSOT-measured ICG half-life occurring at day 2 (236.8 ±35.8 s) compared to sham-operated mice (47.0 ±1.5 s). However, this almost returned to baseline values by day 7 (sFigure 3C). In this model, a strong and significant correlation ($r = 0.78$, P value < 0.0001) was observed between MRI-measured hepatic volume and MSOT-derived ICG clearance measured at the same time in the same mouse Figure 3D). The liver parenchyma did not exhibit any histological changes, neither at the day of surgery nor on day 7 (data not shown).

GSH depletion after APAP challenge confirm APAP bioactivation, hepatotoxicity and strongly correlates with liver function impairment

Throughout this study, the expected early depletion in hepatic glutathione (GSH) induced by APAP followed by its repletion at late time points was observed **(Figure 4A)** (Mitchell *et al.*, 1973). In addition to these, there was also a strong relationship ($r = -0.63$, P value = 0.0007) between APAP-induced GSH depletion and ICG clearance kinetics that also reflected individual mouse responses **(Figure 4B)**.

Relationship between ICG clearance kinetics, circulating biomarkers and histopathological scoring during acetaminophen hepatotoxicity

To evaluate the utility of MSOT-measured ICG clearance in experimental APAP-ILI, we correlated these measurements with quantitative values of circulating mechanistic biomarkers and histopathological measures determined at the same time in the same animal. At early time points post-APAP treatment (3, 6, 24 h), a strong correlation between ICG half-life and all other measured parameters was observed **(Table 1)**. Moreover, a strong correlation with cell injury and death, scored by a pathologist, was also observed at these early time points (3, 6, and 24 h) **(Figure 5)**. At 48 h, the correlation appeared to have disconnected for the circulating biomarkers and ICG clearance **(Table 1)**.

Hepato-protective efficacy of NAC is demonstrated by MSOT measured ICG clearance kinetics and circulating biomarkers

NAC represents an effective antidote to liver injury induced by APAP overdose in patients that present early to hospital (Antoine and Dear, 2016). To investigate the utility of MSOT-measured ICG clearance to assess the efficacy of NAC in experimental APAP hepatotoxicity, we treated mice with NAC 1 h after APAP dosing and measured hepatic function and toxicity at 6 and 24 h post-APAP. NAC prevented the APAP-induced increase in ALT activity and GSH depletion **(Figure 6A,E).** A decrease in ICG half-life at both 6 and 24 h was observed after NAC treatment compared to non-NAC treated APAP intoxicated mice **(Figure 6F)**. These data were also supported by the reduction in the circulating biomarkers in the NAC-treated group when measured at both 6 and 24 h post dosing **(Figure 6B-D)**. The histological examination confirmed the findings **(Figure 6G)**. At 6 h post dosing, there was no evidence of hepatocyte death (median score 0). The only sign of damage was the centrilobular loss of glycogen which was occasionally accompanied by HD of a few

hepatocytes in the innermost centrilobular hepatocyte layer **(Figure 6G)**. At 24 h, the histological changes were similar to those in APAP-dosed mice without NAC treatment, though less severe (median score 1.5) **(Figure 6G)**. These findings suggest a delay and reduction of the damage induced by APAP.

Comparison of the loss of liver function measured by MSOT induced by either acetaminophen hepatotoxicity or resection

Within the individual models of hepatic functional impaired used here (APAP or PH), we observed a strong and significant relationship between ICG clearance and loss of functional parenchyma (APAP: loss of functional parenchyma assessed by histology, PH: loss of absolute liver mass loss assessed by MRI). We now sought to determine the relative relationship between these models for assessing a defined degree of functional liver mass loss that was shown by a qualitative change in MSOT-derived ICG clearance. Supplementary figure 2 illustrates the percentage of liver mass loss determined either by MRI (PH model) or histopathological examination (APAP; 3h and 24h timepoint), that corresponded to the matched MSOT-measured ICG clearance value for the respective models (Supplementary figure 2 **A-B)**. Interestingly, the early degenerative changes (hydropic swelling of centrilobular hepatocytes) at 3 h after APAP overdose had a large impact on ICG clearance kinetics compared to the massive loss of hepatic mass after 60% PH (Supplementary figure 2 **A)** and the extensive centrilobular necrosis present at 24 h post dosing (Supplementary figure 2 **B**). At this time point, the PH model demonstrated significantly lower hepatic function than the liver injury induced by APAP when determined by ICG clearance (Supplementary figure 2 **B)**.

DISCUSSION

Here, for the first time, we report the utility of non-invasive photoacoustic imaging and its assimilation with circulating mechanistic biomarkers and traditional methods for evaluating hepatic integrity to investigate the onset and recovery from experimental acute liver injury using APAP as a paradigm. This "tool box" approach can be used to assess the impact of ALI at both the whole organ and hepatocellular level, longitudinally, in the same animal. Our findings reveal a strong and statistically significant relationship between the novel and traditional biomarkers of hepatic injury, histopathological assessments and functional ICG clearance measured by MSOT. These observations provide evidence for the integrated use of these parameters to deliver added value and a new dynamic for the preclinical assessment of experimental ALI that has potential translational application.

A significant novel aspect to this current report is the assessment of hepatic function, in a non-invasive way, by utilising MSOT to measure ICG clearance. MSOT analysis permitted the extent of hepatic degeneration and regeneration to be monitored in individual mice repeatedly. Here we have used two distinct models that have direct clinical relevance and perturb the liver at either the cellular or whole organ level. Previous studies have demonstrated the accuracy and reliability of the measurements of ICG kinetics for the assessment of liver function in different conditions such as liver transplantation or partial resection, amongst others (Imamura *et al.*, 2005; Levesque *et al.*, 2016; Pinzani, 2016). The ICG clearance test is a qualitative liver function test used during clinical liver surgery and transplantation (Breitenstein *et al.*, 2009; de Graaf *et al.*, 2010) and has already been used as a prognostic tool to predict

survival in sepsis and acute liver failure as well as in critically ill patients (Halle *et al.*, 2014). For instance, the early non-invasive measurement of ICG was demonstrated to accurately predict severe graft dysfunction and mortality after liver transplantation (Faybik and Hetz, 2006; Olmedilla *et al.*, 2009). The delay in ICG clearance has been explained by a loss in hepatocyte content which consequently reduces the capacity of the liver to uptake this compound and excrete it into the gall bladder. A number of different techniques have been used to measure ICG and have been associated with significant limitations such as cost, time, number of required blood samples and invasiveness (Halle *et al.*, 2014; Levesque *et al.*, 2016). Moreover, these limitations are further exaggerated when considering the preclinical assessment of hepatic impairment. Therefore, the approach we have used offers a significant advantage by allowing a real-time and non-invasive measurement of hepatic function in the same animal and in a longitudinal manner that correlates with circulating biomarkers of liver injury and the histopathological assessment of damage. The multiplicity of techniques can be utilised simultaneously to provide different but complementary readouts that inform on experimental APAP-ILI in a sensitive and specific manner.

Despite the relative advantages of this approach, it is important to note that this strategy is not without limitation. The filtration of ICG is dependent upon blood flow (Levesque *et al.*, 2016) and it has been reported that the APAP-ILI model can lead to haemodynamic changes (Randle *et al.*, 2008). Therefore, in order to determine that our observations regarding ICG kinetics were not misrepresented, we measured the blood velocity at 6 and 24 h after APAP treatment using ultrasound and Doppler technology (data not shown). Here, no differences in blood velocity were observed following APAP treatment in mice compared to controls. This does, however, not

exclude that the hydropic swelling of centrilobular hepatocytes at 3 h post APAP might have impaired the blood flow at that particular time point. Also, clearance from the liver into the gall bladder is known to depend on ATP-dependent transport proteins such as ATP-binding cassettes (ABC) (Mrp2 and Mdr2 in mice) (Shinohara *et al.*, 1996; Huang and Vore, 2001) and these transporters are known to be up- or down-regulated after single or chronic dosing of APAP (Aleksunes *et al.*, 2005; Aleksunes *et al.*, 2008). Therefore, it is conceivable that this could impact on data interpretation. However, Aleksunes *et al* (2005) only observed significant up- or down-regulation of these transporters at a dose of 400 mg/kg and not at 300 mg/kg. Our study has only focused on the acute treatment of mice with APAP (300 mg/kg) and we have demonstrated that the measurement of ICG in blood, rather than from the gall bladder, does produce robust and reproducible results and correlates with mechanistic circulating biomarkers of liver injury. Moreover, the uptake from the liver parenchyma is known to be led by non-ATP dependent transporters such as organic anion transporters polypeptides (OATP) and Na^+-taurocholate co-transporting polypeptides (NTCP) (Berk and Stremmel, 1986; de Graaf *et al.*, 2011). Therefore, taking into account these factors and the strong association between ICG clearance and blood-based biomarkers of toxicity and histopathology, we conclude that our data can be interpreted as a result of a decreased capacity of the liver to uptake and clear this dye. The most likely explanation for it is a significant loss of the number of functional hepatocytes as a result of the toxic effect of APAP.

To a greater extent, ICG clearance reflected liver function fluctuations across the time course which was imperceptible by the serum biomarkers but was mirrored by histological features. An increase of glycogen storage in the hepatocytes from the undamaged area was reproduced by a liver function recovery at 24 h time point post-

APAP challenge and the inflammatory response, the ongoing cell death and functional hepatic mass loss histologically described amongst other features was seen as a second peak of liver function impairment at 48 h. Additionally, the disconnection of the serum biomarker and ICG half-life correlation also demonstrates the utility of the individual parameters in combination and added value that liver function measurement adds to the understanding of this phenomenon. This can be rationalized by the variability and characteristics of the different biomarkers, such as their half-life or time/mechanism of release in the circulation (Giannini *et al.*, 2005).

The PH model used in this study provided mechanistic insights allowing a better understanding and validation of the ICG half-life parameter used as a metric of liver function in the onset of APAP induced acute liver injury. Centrilobular cell death has been widely reported previously in rodents and humans, with APAP-induced hepatotoxicity causing localised, i.e. zonal (centrilobular) hepatocyte death and representing a loss of hepatocytes with a specific phenotype and therefore liver function (Oinonen and Lindros, 1998; Gujral *et al.*, 2002). This particular type of liver function impairment is not reproduced with the PH model in which an entire lobe is removed, thereby preserving the integrity of the remaining functional liver. This is further demonstrated at early time points post-APAP treatment, in which liver function appears to be severely impaired (high ICG half-life values) compared to the PH model (Supplementary figure 1 **A)**. At 24 h after APAP treatment, the ICG clearance is near basal levels despite sustained necrosis (i.e. effective hepatocytes loss) and we could see low ICG half-life values compared to the PH model (Supplementary figure 1 **B)**. As mentioned previously this is potentially as a result of the compensatory functional response of the unaffected lobular regions (regional increase of glycogen storage and GSH levels). The unaffected areas can therefore

compensate the metabolic and functional needs of the liver thereby enabling survival. Photoacoustic imaging could therefore hold the potential to classify specific types of damage related to discrete injury types, non-invasively, when used alongside a panel of mechanistic circulating biomarkers.

In conclusion, using APAP as a paradigm, this study demonstrates for the first time that the integration of novel non-invasive and dynamic imaging markers of hepatic function with mechanistic circulating biomarkers of hepatotoxicity, alongside traditional histopathological evaluation, can provide a new way to assess experimental hepatotoxicity and its pharmacological restoration that has translational potential.

ACKNOWLEDGMENTS

The authors would like to acknowledge the financial support from the Medical Research Council (MRC) Integrative Toxicology Training Programme (ITTP) and the United Kingdom Regenerative Medicine Platform (UKRMP) Safety and Efficacy Hub (Ref: MR/K026739/1). Imaging data were obtained in the Centre for Preclinical Imaging (CPI) of the University of Liverpool. The CPI has been funded by a Medical Research Council (MRC) grant (MR/L012707/1). We would also like to thank the technical staff in the Histology Laboratory, Veterinary Laboratory Services, Institute of Veterinary Science, University of Liverpool, for excellent technical support.

REFERENCES

Aleksunes, L.M., Campion, S.N., Goedken, M.J., Manautou, J.E., 2008. Acquired resistance to acetaminophen hepatotoxicity is associated with induction of multidrug resistance-associated protein 4 (Mrp4) in proliferating hepatocytes. Toxicological sciences : an official journal of the Society of Toxicology **104**, 261-273.

Aleksunes, L.M., Slitt, A.M., Cherrington, N.J., Thibodeau, M.S., Klaassen, C.D., Manautou, J.E., 2005. Differential expression of mouse hepatic transporter genes in response to acetaminophen and carbon tetrachloride. Toxicological sciences : an official journal of the Society of Toxicology **83**, 44-52.

Antoine, D.J., Dear, J.W., 2016. How to treat paracetamol overdose and when to do it. Expert review of clinical pharmacology **9**, 633-635.

Antoine, D.J., Dear, J.W., 2017. Transformative biomarkers for drug-induced liver injury: are we there yet? Biomark Med **11**, 103-106.

Antoine, D.J., Dear, J.W., Lewis, P.S., Platt, V., Coyle, J., Masson, M., Thanacoody, R.H., Gray, A.J., Webb, D.J., Moggs, J.G., Bateman, D.N., Goldring, C.E., Park, B.K., 2013. Mechanistic biomarkers provide early and sensitive detection of acetaminophen-induced acute liver injury at first presentation to hospital. Hepatology (Baltimore, Md.) **58**, 777-787.

Antoine, D.J., Jenkins, R.E., Dear, J.W., Williams, D.P., McGill, M.R., Sharpe, M.R., Craig, D.G., Simpson, K.J., Jaeschke, H., Park, B.K., 2012. Molecular forms of HMGB1 and keratin-18 as mechanistic biomarkers for mode of cell death and prognosis during clinical acetaminophen hepatotoxicity. Journal of hepatology **56**, 1070-1079.

Antoine, D.J., Williams, D.P., Kipar, A., Jenkins, R.E., Regan, S.L., Sathish, J.G., Kitteringham, N.R., Park, B.K., 2009. High-mobility group box-1 protein and keratin-18, circulating serum proteins informative of acetaminophen-induced necrosis and apoptosis in vivo. Toxicological sciences : an official journal of the Society of Toxicology **112**, 521-531.

Antoine, D.J., Williams, D.P., Kipar, A., Laverty, H., Park, B.K., 2010. Diet restriction inhibits apoptosis and HMGB1 oxidation and promotes inflammatory cell recruitment during acetaminophen hepatotoxicity. Mol Med **16**, 479-490.

Berk, P.D., Stremmel, W., 1986. Hepatocellular uptake of organic anions. Prog Liver Dis **8**, 125-144.

Bradford, M.M., 1976. A rapid and sensitive method for the quantitation of microgram quantities of protein utilizing the principle of protein-dye binding. Analytical biochemistry **72**, 248-254.

Breitenstein, S., Dimitroulis, D., Petrowsky, H., Puhan, M.A., Mullhaupt, B., Clavien, P.A., 2009. Systematic review and meta-analysis of interferon after curative treatment of hepatocellular carcinoma in patients with viral hepatitis. The British journal of surgery **96**, 975-981.

Clarke, J.I., Dear, J.W., Antoine, D.J., 2016. Recent advances in biomarkers and therapeutic interventions for hepatic drug safety - false dawn or new horizon? Expert opinion on drug safety **15**, 625-634.

de Graaf, W., Bennink, R.J., Vetelainen, R., van Gulik, T.M., 2010. Nuclear imaging techniques for the assessment of hepatic function in liver surgery and transplantation. Journal of nuclear medicine : official publication, Society of Nuclear Medicine **51**, 742-752.

de Graaf, W., Hausler, S., Heger, M., van Ginhoven, T.M., van Cappellen, G., Bennink, R.J., Kullak-Ublick, G.A., Hesselmann, R., van Gulik, T.M., Stieger, B., 2011. Transporters involved in the hepatic uptake of (99m)Tc-mebrofenin and indocyanine green. Journal of hepatology **54**, 738-745.

Dima, A., Burton, N.C., Ntziachristos, V., 2014. Multispectral optoacoustic tomography at 64, 128, and 256 channels. J Biomed Opt **19**, 36021.

Eakins, R., Walsh, J., Randle, L., Jenkins, R.E., Schuppe-Koistinen, I., Rowe, C., Starkey Lewis, P., Vasieva, O., Prats, N., Brillant, N., Auli, M., Bayliss, M., Webb, S., Rees, J.A., Kitteringham, N.R., Goldring, C.E., Park, B.K., 2015. Adaptation to acetaminophen exposure elicits major changes in expression and distribution of the hepatic proteome. Scientific reports **5**, 16423.

EMA, 2016. http://www.ema.europa.eu/docs/en_GB/document_library/Other/2016/09/WC500213479.pdf.

Faybik, P., Hetz, H., 2006. Plasma disappearance rate of indocyanine green in liver dysfunction. Transplant Proc **38**, 801-802.

FDA, 2016. http://www.fda.gov/Drugs/DevelopmentApprovalProcess/ucm434382.htm.

Giannini, E.G., Testa, R., Savarino, V., 2005. Liver enzyme alteration: a guide for clinicians. CMAJ : Canadian Medical Association journal = journal de l'Association medicale canadienne **172**, 367-379.

Gujral, J.S., Knight, T.R., Farhood, A., Bajt, M.L., Jaeschke, H., 2002. Mode of cell death after acetaminophen overdose in mice: apoptosis or oncotic necrosis? Toxicological sciences : an official journal of the Society of Toxicology **67**, 322-328.

Halle, B.M., Poulsen, T.D., Pedersen, H.P., 2014. Indocyanine green plasma disappearance rate as dynamic liver function test in critically ill patients. Acta anaesthesiologica Scandinavica **58**, 1214-1219.

Huang, L., Vore, M., 2001. Multidrug resistance p-glycoprotein 2 is essential for the biliary excretion of indocyanine green. Drug Metab Dispos **29**, 634-637.

Imamura, H., Sano, K., Sugawara, Y., Kokudo, N., Makuuchi, M., 2005. Assessment of hepatic reserve for indication of hepatic resection: decision tree incorporating indocyanine green test. J Hepatobiliary Pancreat Surg **12**, 16-22.

Levesque, E., Martin, E., Dudau, D., Lim, C., Dhonneur, G., Azoulay, D., 2016. Current use and perspective of indocyanine green clearance in liver diseases. Anaesth Crit Care Pain Med **35**, 49-57.

Lundback, P., Lea, J.D., Sowinska, A., Ottosson, L., Furst, C.M., Steen, J., Aulin, C., Clarke, J.I., Kipar, A., Klevenvall, L., Yang, H., Palmblad, K., Park, B.K., Tracey, K.J., Blom, A.M., Andersson, U., Antoine, D.J., Erlandsson Harris, H., 2016. A novel high mobility group box 1 neutralizing chimeric antibody attenuates drug-induced liver injury and postinjury inflammation in mice. Hepatology (Baltimore, Md.) **64**, 1699-1710.

McGill, M.R., Sharpe, M.R., Williams, C.D., Taha, M., Curry, S.C., Jaeschke, H., 2012. The mechanism underlying acetaminophen-induced hepatotoxicity in humans and mice involves mitochondrial damage and nuclear DNA fragmentation. The Journal of clinical investigation **122**, 1574-1583.

McNally, L.R., Mezera, M., Morgan, D.E., Frederick, P.J., Yang, E.S., Eltoum, I.E., Grizzle, W.E., 2016. Current and Emerging Clinical Applications of Multispectral Optoacoustic Tomography (MSOT) in Oncology. Clinical cancer research : an official journal of the American Association for Cancer Research **22**, 3432-3439.

Mitchell, J.R., Jollow, D.J., Potter, W.Z., Gillette, J.R., Brodie, B.B., 1973. Acetaminophen-induced hepatic necrosis. IV. Protective role of glutathione. J Pharmacol Exp Ther **187**, 211-217.

Morscher, S., Driessen, W.H., Claussen, J., Burton, N.C., 2014. Semi-quantitative Multispectral Optoacoustic Tomography (MSOT) for volumetric PK imaging of gastric emptying. Photoacoustics **2**, 103-110.

Oinonen, T., Lindros, K.O., 1998. Zonation of hepatic cytochrome P-450 expression and regulation. The Biochemical journal **329 (Pt 1)**, 17-35.

Olmedilla, L., Perez-Pena, J.M., Ripoll, C., Garutti, I., de Diego, R., Salcedo, M., Jimenez, C., Banares, R., 2009. Early noninvasive measurement of the indocyanine green plasma disappearance rate accurately predicts early graft dysfunction and mortality after deceased donor liver transplantation. Liver Transpl **15**, 1247-1253.

Owens, C.W., Belcher, R.V., 1965. A COLORIMETRIC MICRO-METHOD FOR THE DETERMINATION OF GLUTATHIONE. The Biochemical journal **94**, 705-711.

Pinzani, A.M.a.M., 2016. The Holy Grail of a Biomarker for "Liver Function". Clinical liver disease **7**, 135-138.

Randle, L.E., Sathish, J.G., Kitteringham, N.R., Macdonald, I., Williams, D.P., Park, B.K., 2008. alpha(1)-Adrenoceptor antagonists prevent paracetamol-induced hepatotoxicity in mice. British journal of pharmacology **153**, 820-830.

Reuben, A., Tillman, H., Fontana, R.J., Davern, T., McGuire, B., Stravitz, R.T., Durkalski, V., Larson, A.M., Liou, I., Fix, O., Schilsky, M., McCashland, T., Hay, J.E., Murray, N., Shaikh, O.S., Ganger, D., Zaman, A., Han, S.B., Chung, R.T., Smith, A., Brown, R., Crippin, J., Harrison, M.E., Koch, D., Munoz, S., Reddy, K.R., Rossaro, L., Satyanarayana, R., Hassanein, T., Hanje, A.J., Olson, J., Subramanian, R., Karvellas, C., Hameed, B., Sherker, A.H., Robuck, P., Lee, W.M., 2016. Outcomes in Adults With Acute Liver Failure Between 1998 and 2013: An Observational Cohort Study. Ann Intern Med **164**, 724-732.

Riehle, K.J., Dan, Y.Y., Campbell, J.S., Fausto, N., 2011. New concepts in liver regeneration. Journal of gastroenterology and hepatology **26 Suppl 1**, 203-212.

Sakka, S.G., 2007. Assessing liver function. Curr Opin Crit Care **13**, 207-214.

Sakka, S.G., Reinhart, K., Meier-Hellmann, A., 2002. Prognostic value of the indocyanine green plasma disappearance rate in critically ill patients. Chest **122**, 1715-1720.

Scarfe, L., Rak-Raszewska, A., Geraci, S., Darssan, D., Sharkey, J., Huang, J., Burton, N.C., Mason, D., Ranjzad, P., Kenny, S., Gretz, N., Levy, R., Kevin Park, B., Garcia-Finana, M., Woolf, A.S., Murray, P., Wilm, B., 2015. Measures of kidney function by minimally invasive techniques correlate with histological glomerular damage in SCID mice with adriamycin-induced nephropathy. Scientific reports **5**, 13601.

Shinohara, H., Tanaka, A., Kitai, T., Yanabu, N., Inomoto, T., Satoh, S., Hatano, E., Yamaoka, Y., Hirao, K., 1996. Direct measurement of hepatic indocyanine green clearance with near-infrared spectroscopy: separate evaluation of uptake and removal. Hepatology (Baltimore, Md.) **23**, 137-144.

Starkey Lewis, P.J., Dear, J., Platt, V., Simpson, K.J., Craig, D.G., Antoine, D.J., French, N.S., Dhaun, N., Webb, D.J., Costello, E.M., Neoptolemos, J.P., Moggs, J., Goldring, C.E., Park, B.K., 2011. Circulating microRNAs as potential markers of human drug-induced liver injury. Hepatology **54**, 1767-1776.

Stoffels, I., Morscher, S., Helfrich, I., Hillen, U., Leyh, J., Burton, N.C., Sardella, T.C., Claussen, J., Poeppel, T.D., Bachmann, H.S., Roesch, A., Griewank, K., Schadendorf, D., Gunzer, M., Klode, J., 2015. Metastatic status of sentinel lymph nodes in melanoma determined noninvasively with multispectral optoacoustic imaging. Science translational medicine **7**, 317ra199.

Stutchfield, B.M., Antoine, D.J., Mackinnon, A.C., Gow, D.J., Bain, C.C., Hawley, C.A., Hughes, M.J., Francis, B., Wojtacha, D., Man, T.Y., Dear, J.W., Devey, L.R., Mowat, A.M., Pollard, J.W., Park, B.K., Jenkins, S.J., Simpson, K.J., Hume, D.A., Wigmore, S.J., Forbes, S.J., 2015. CSF1 Restores Innate Immunity After Liver Injury in Mice and Serum Levels Indicate Outcomes of Patients With Acute Liver Failure. Gastroenterology **149**, 1896-1909 e1814.

Tannapfel, A., Dienes, H.P., Lohse, A.W., 2012. The indications for liver biopsy. Deutsches Arzteblatt international **109**, 477-483.

Taruttis, A., Timmermans, A.C., Wouters, P.C., Kacprowicz, M., van Dam, G.M., Ntziachristos, V., 2016. Optoacoustic Imaging of Human Vasculature: Feasibility by Using a Handheld Probe. Radiology **281**, 256-263.

Waldner, M.J., Knieling, F., Egger, C., Morscher, S., Claussen, J., Vetter, M., Kielisch, C., Fischer, S., Pfeifer, L., Hagel, A., Goertz, R.S., Wildner, D., Atreya, R., Strobel, D., Neurath, M.F., 2016. Multispectral Optoacoustic Tomography in Crohn's Disease: Noninvasive Imaging of Disease Activity. Gastroenterology **151**, 238-240.

Wang, K., Zhang, S., Marzolf, B., Troisch, P., Brightman, A., Hu, Z., Hood, L.E., Galas, D.J., 2009. Circulating microRNAs, potential biomarkers for drug-induced liver injury. Proc Natl Acad Sci U S A **106**, 4402-4407.

Wang, X., Pang, Y., Ku, G., Xie, X., Stoica, G., Wang, L.V., 2003. Noninvasive laser-induced photoacoustic tomography for structural and functional in vivo imaging of the brain. Nature biotechnology **21**, 803-806.

Wheeler, H.O., Cranston, W.I., Meltzer, J.I., 1958. Hepatic uptake and biliary excretion of indocyanine green in the dog. Proc Soc Exp Biol Med **99**, 11-14.

Williams, D.P., Antoine, D.J., Butler, P.J., Jones, R., Randle, L., Payne, A., Howard, M., Gardner, I., Blagg, J., Park, B.K., 2007. The metabolism and toxicity of furosemide in the Wistar rat and CD-1 mouse: a chemical and biochemical definition of the toxicophore. J Pharmacol Exp Ther **322**, 1208-1220.

Zhang, H.F., Maslov, K., Stoica, G., Wang, L.V., 2006. Functional photoacoustic microscopy for high-resolution and noninvasive in vivo imaging. Nature biotechnology **24**, 848-851.

FIGURE AND TABLE LEGENDS

Table 1. Correlation between circulating biomarkers and ICG kinetics during APAP-induced hepatotoxicity in mice. ICG half-life and biomarkers measured after APAP challenge at 3 and 6 h strongly correlate with a noticeable disconnection at 24 and 48 h for ALT, TBIL, miR-122 and HMGB1. Complete disconnection at 72 and 96 h. Data represents the correlation coefficient r (P value) from the analysis of both saline control and APAP treated mice (n = 6-10 per treatment per time point).

Time	Circulating biomarker			
	ALT	**TBIL**	**miR-122**	**HMGB1**
3	0.74 (0.004)	0.80 (0.0009)	0.62 (0.02)	0.82 (0.0006)
6	0.76 (0.002)	0.53 (0.05)	0.70 (0.005)	0.56 (0.04)
24	0.49 (0.06)	0.60 (0.02)	0.03 (0.92)	0.73 (0.004)
48	0.07 (0.85)	0.17 (0.63)	0.07 (0.85)	0.0 (0.55)
72	0.76 (0.01)	0.21 (0.55)	0.32 (0.36)	0.63 (0.05)
96	0 (0.93)	0.46 (0.22)	0 (0.74)	0 (0.84)

Figure 1. Plasma biomarker levels and type and degree of histological changes observed during APAP-induced hepatotoxicity in mice. Mice were administered with APAP (300 mg/kg) and monitored at 3, 6, 24, 48, 72 and 96 h after dosing. (A) ALT increased significantly early and progressively up to 24 h in the serum of APAP-

overdosed mice compared to saline treated (control) mice, (B) TBIL increased early significantly in the serum of APAP-overdosed mice and remained elevated compared to non-treated mice, (C) miR-122 increased significantly early and progressively up to 6 h in the serum of APAP-overdosed mice compared to non-treated mice. (D) After an early significant increase in total HMGB1 in the serum of APAP-overdosed mice compared to non-treated mice values decreased progressively. (A-D) Bars represent mean ± standard error of the mean of group of animals (black = control, n = 4-6; white = APAP overdose, n = 6-10). Asterisks indicate significance of two-sample t-tests: $p \leq 0.05$ (*), $p \leq 0.005$ (**), $p \leq 0.0005$ (***)**.**

(E) Representative HE-stained liver sections from saline treated mice (controls) and mice after APAP overdose (3, 6, 24, 48, 72, and 96 h post dosing). At 3 h post APAP, the main finding is centrilobular loss of glycogen and HD of hepatocytes in the innermost layers (arrows). At 6 and 24 h, centrilobular coagulative necrosis of several hepatocyte layers is seen (breadth of necrosis indicated by black line). At 6 h, hepatocytes outside affected areas are entirely devoid of glycogen, at 24 h, only 1-2 hepatocyte layers surrounding the necrotic hepatocytes are devoid of glycogen (breadth indicated by short black line), and glycogen has been restituted in the remaining parenchyma. At 48 h, the innermost centrilobular areas are comprised of (new) glycogen-free hepatocytes intermingled with individual necrotic hepatocytes (arrows). At 72 h, there is no evidence of cell death, but centrilobular areas appear less cellular than in controls. The presence of mitotic cells (arrows) indicates regeneration. At 96 h, centrilobular areas are more cellular, and there is mild leukocyte infiltration around the central vein (arrows). CV = central vein. Bars = 20 µm.

Figure 2. Parametric maps and quantification of MSOT kinetics. Panels A and B show parametric maps for a control mouse (A) and an APAP treated mouse (B), where kinetic modelling was performed on a per pixel basis. The elimination rate constant is shown in jet as an overlay on a 900nm MSOT image. Blue jet colour expresses a low rate constant (K) representative of liver function impairment. Contrarily, red pixels describes normal clearance rate of ICG. Pixels which fit poorly within the ROI were excluded from the analysis and therefore transparent. The left (red) and right (green) ischiatic vessels are shown, as well as vessels surrounding the caudal vertebra (orange). Panels C (control) and D (6h time point post-APAP) show quantification of spectrally unmixed ICG MSOT signal within the left ischiatic vessel. Raw MSOT data was modelled using a single exponential algorithm and shown in red in the graph. The average rate constant (K) and half-life ($t_{1/2}$) for the entire ROI is shown as an inset on the graph. Mice were administered with APAP (300 mg/kg) and monitored at 3, 6, 24, 48, 72 and 96 h after dosing. (E) Significant increase in ICG half-life after APAP-overdose compared to untreated mice up to 72 h, and return to baseline values at 96 h. Bars represent mean ± standard error of the mean of group of animals (black = control, n = 4-6; white = APAP (300 mg/kg) overdose, n = 6-10). (C) Decrease in rate constant after APAP-overdose during the monitoring of liver function. (C) Bars represent mean ± standard error of the mean of group of animals (n = 5). Asterisks indicate significance in two-sample t-tests: $p \leq 0.05$ (*), $p \leq 0.005$ (**).

Figure 3: Relationship between hepatic mass measured by MRI and hepatic function measured by MSOT following partial hepatectomy in mice. Mice underwent 60 % hepatectomy or sham surgery and were examined 1, 2, 3 and 7 days after surgery. (A) MRI images from a mouse before and after liver resection. (B)

Average of liver mass recovery after 60 % hepatectomy from 5 mice during the days after surgery. (C) ICG half-life measurements after sham operation and 60 % hepatectomy. Bars represent mean ± standard error of the mean of group of animals (*n*=5). Asterisks indicate significance in two-sample t-tests: $p \leq 0.05$ (*), $p \leq 0.005$ (**). (D) Scatterplot showing a correlation coefficient of 60 % ($r = 0.78$, P value < 0.0001) hepatectomy cohort data between the percentage of liver mass loss and the ICG half-life from the ischiatic vessels measurements. Data points represent individual animals (triangles = 60 % hepatectomy, $n = 5$, day 0, 1, 2, 3 and 7 after surgery). Trend line for 60 % hepatectomy animals is displayed.

Figure 4: Glutathione measurements after APAP overdose and its correlation with ICG kinetics. (A) GSH levels in control compared to APAP treated mice at 3, 6, 24, 48, 72 and 96 h post injection and (B) correlation between GSH levels from different time points and ICG half-life ($r = -0.63$, P value = 0.0007). (A) Bars represent mean ± standard error of the mean of group of animals (black = control, $n = 5$; white = APAP (300 mg/kg) overdose, $n = 5$). Asterisks indicate significance of two-sample t-tests: $p \leq 0.05$ (*), $p \leq 0.005$ (**).

Figure 5. Correlation between histopathology score and ICG kinetics during APAP-induced hepatotoxicity in mice. The degree of liver degeneration and necrosis/cell loss statistically significantly correlates with the delay of ICG clearance at 3 h (A), 6 h (B) and 24 h (C) post treatment, however at 48 h (D) this correlation is much lower. (E) By 72 h, the ICG clearance has almost returned to control animal values, and at 96 h the values in treated and control animals are at the same level.

Data points represent individual animals (circles = control, *n* = 4-5; triangles = APAP-administered, *n* = 6-9).

Figure 6. Impact of NAC on APAP-induced changes in circulating biomarkers and ICG kinetics in mice. Mice were administered with APAP (300 mg/kg) and received NAC at 1 h post APAP. They were examined at 6 h and 24 h after APAP dosing. (A) ALT, (B) TBIL, (C) miR-122 and (D) total HMGB1 serum levels decreased in NAC-treated mice compared to non-treated mice. An increase in (E) GSH levels in hepatocytes parenchyma anda decrease in (F) ICG half-life was seen after NAC treatment relative to APAP-treated mice that did not receive NAC. (G) No necrosis was described in the CV area at 6h after NAC treatment and decrease of CV necrosis was seen after 24h. (A-F) Bars represent mean ± standard error of the mean of group of animals (black = control, *n* = 4-6; white = APAP (300 mg/kg) overdose, *n* = 5-10). Asterisks indicate significance in two-sample one way ANOVA (Tukey), control vs APAP overdose groups: $p \leq 0.05$ (*), $p \leq 0.005$ (**), $p \leq 0.0005$ (***), $p \leq 0.0001$ (****), and hash indicate significance in two-sample on way ANOVA (Tukey), APAP overdose vs NAC treated groups $p \leq 0.05$ (#), $p \leq 0.005$ (##), $p \leq 0.0005$ (###), $p \leq 0.0001$ (####) .

SUPPLEMENTARY MATERIAL AND METHODS

Dynamic contrast enhanced (DCE) MSOT image generation

DCE images were generated using a custom-written pharmacokinetic (PK) analysis tool from iThera Medical. A PK model was fitted to image data using an optimization routine to minimize the sum of square error between the model-prediction and the data. Based on the assumption of single-phase elimination of _(ICG)_ via _(liver clearance)_ pathway, a single exponential decay model was used:

$$Y(t) = (Y_0 - Y_{SS})e^{-k*t} + Y_{SS}$$

Fitting was run on a per-pixel basis to provide a parametric map of anatomically-selected ROIs within the image. Pixels in the DCE image were excluded based on a goodness of fit criterion, where pixels yielding an R2 < 0.02 were excluded from the DCE image to improve the confidence of values represented in the image. The final DCE image is represented as the respective parametric map as an overlay on top of representative 900 nm image.

Magnetic resonance imaging (MRI)

Magnetic resonance imaging (MRI) studies were performed with a 9.4T Bruker Biospec 94/20 MRI scanner using a 78 mm body coil transmit and a four-channel receive array coil (Bruker Biospin, Inc.). Mice from the PH study were scanned the day before surgery and on day 1, 2, 3 and 7 after PH. Mice were anesthetised with 1.0–2.0 % isoflurane delivered in 1 L/min oxygen gas ventilation before being placed on a bed where probes for monitoring rectal temperature and respiration were connected to their body. A water-circulating heating pad was placed over the body to

maintain a constant temperature of 37 °C during experiments. At the end of scanning, the mouse was removed from the scanner, and transferred to the MSOT holder device. A T2_TurboRARE MRI sequence was used to acquire the images covering the liver in the coronal plane with the following parameters: TR/TE = 2500/24; echo train length=8; pixel bandwidth = 446.43; averages = 3; field of view = 30x28 mm; slice thickness = 500 µm; slice gap = 100 µm; and in-plane resolution = 125x125 µm. The liver in MR images was segmented using ImageJ for liver volume measurements.

SUPPLEMENTARY FIGURES

Supplementary Figure 1. Score for drug-induced liver injury and degenerative changes. This figure illustrates the features taken into account for the scoring of liver necrosis and hepatocytes undergoing hydropic degeneration.

Supplementary figure 2. Comparison of the relationship between hepatic mass/the extent of liver injury and hepatic function in hepatectomised and APAP-overdosed mice. Scatterplot showing a correlation coefficient of the 60 % hepatectomy cohort data between the liver mass loss (%) and ICG half-life measurements and the correlation coefficient between the APAP-overdosed mice score for (A) degenerative changes at 3 h post APAP dosing (r = 0.89, P value = 0.001) and (B) necrosis at 24 h post dosing (r = 0.63, P value = 0.01) and ICG half-life measurements. Data points represent individual animals (circles = 60 % hepatectomy, *n* = 5, day 1, 2, 3 and 7 after surgery; triangles = APAP-overdosed mice, n = 8-10).

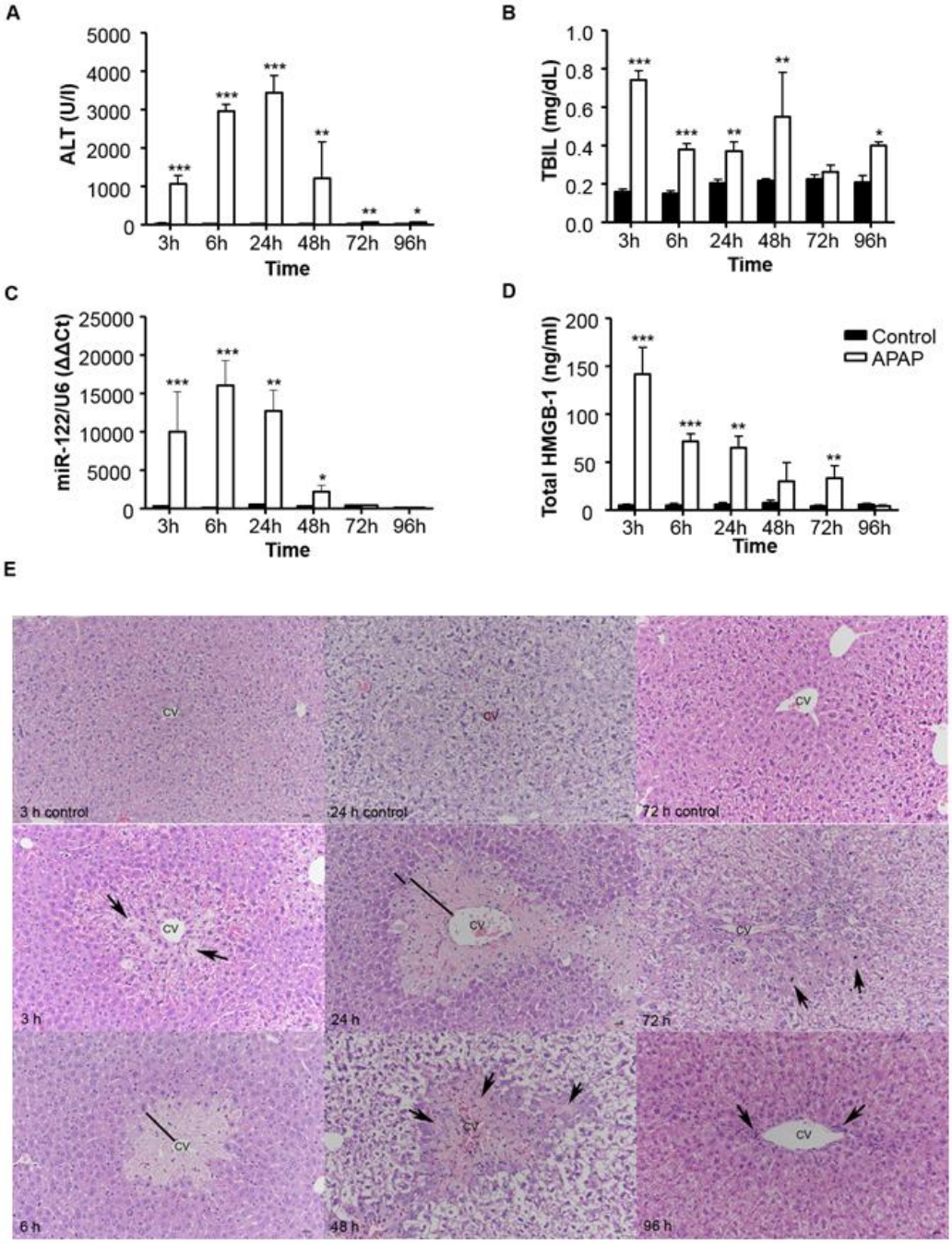

Figure 1

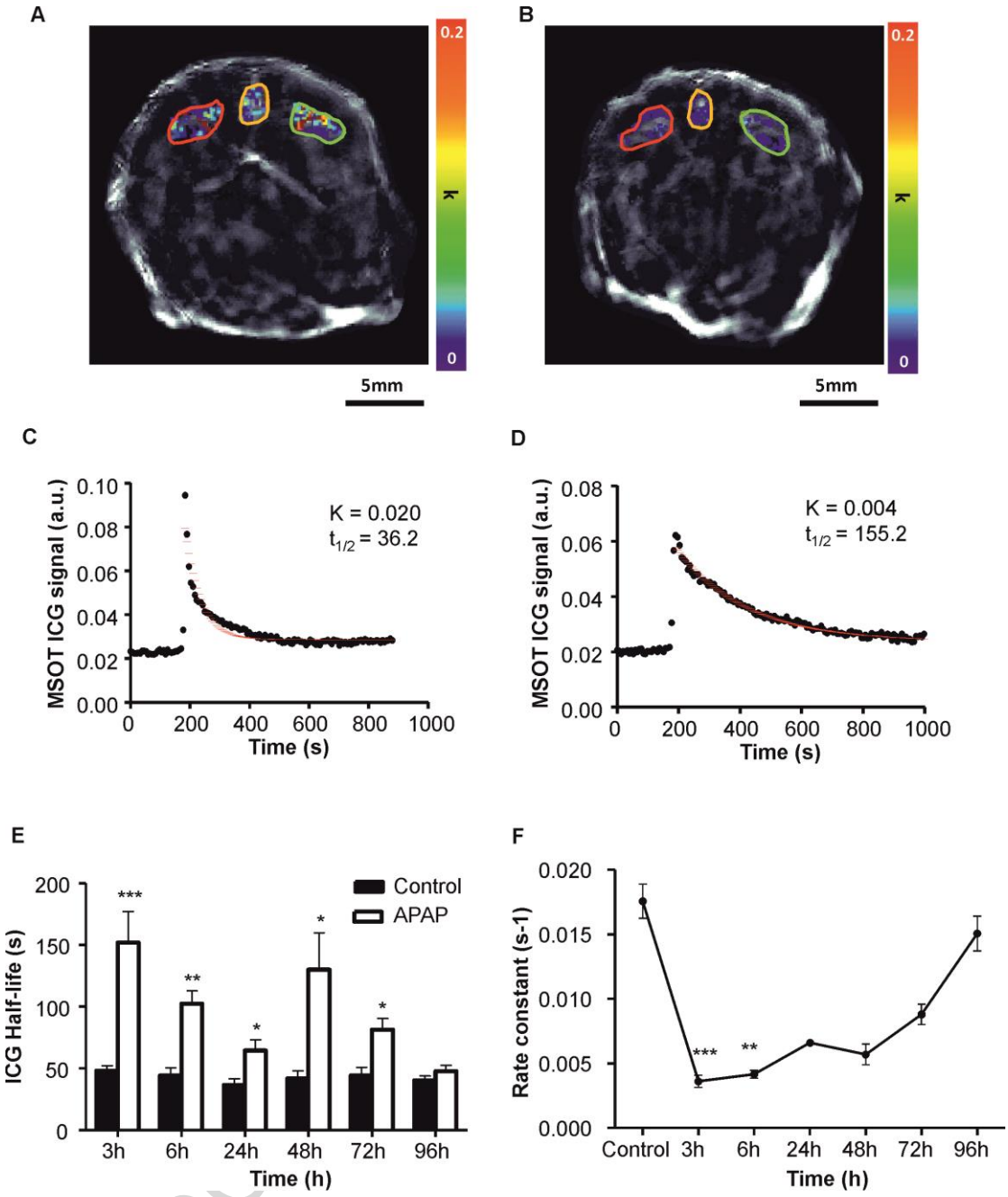

Figure 2

A

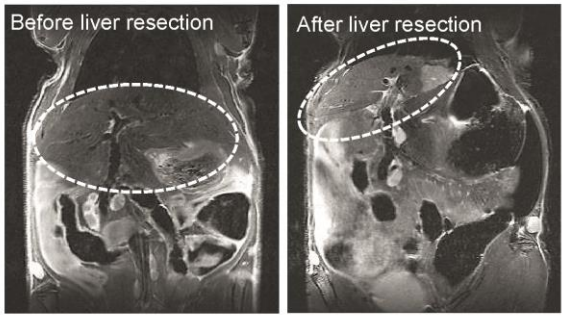

B

Functional liver (%) – MRI data	
Day 0	100%
Surgery	57% removed
Day 1	43%
Day 2	48%
Day 3	62%
Day 7	84%

C

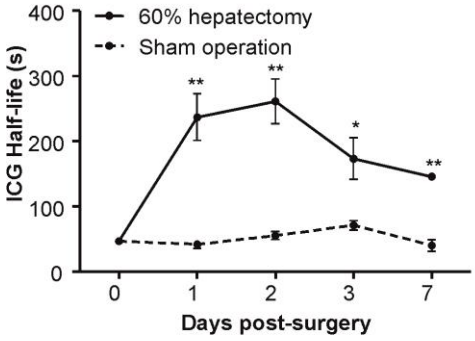

D

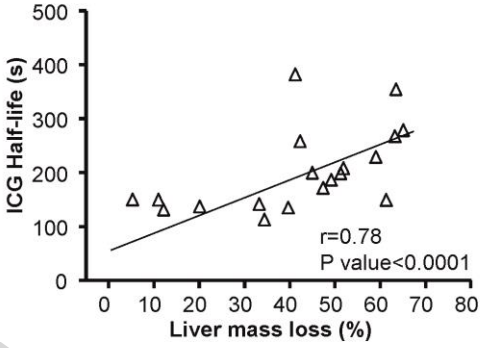

Figure 3

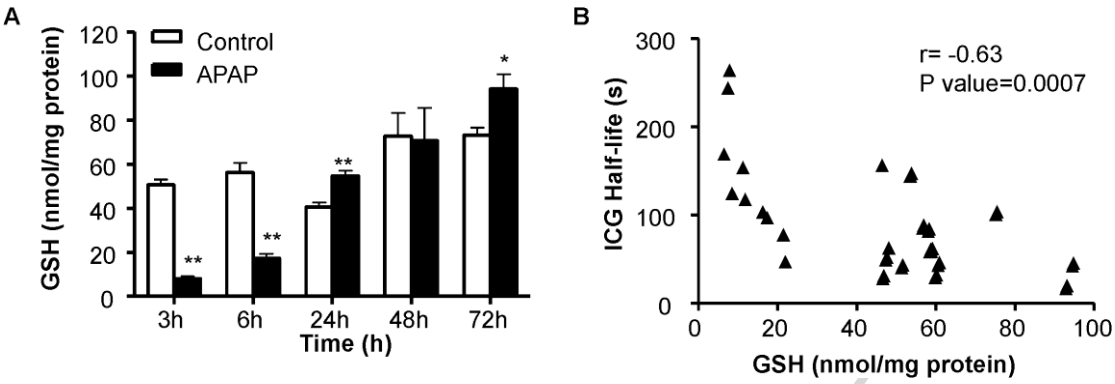

Figure 4

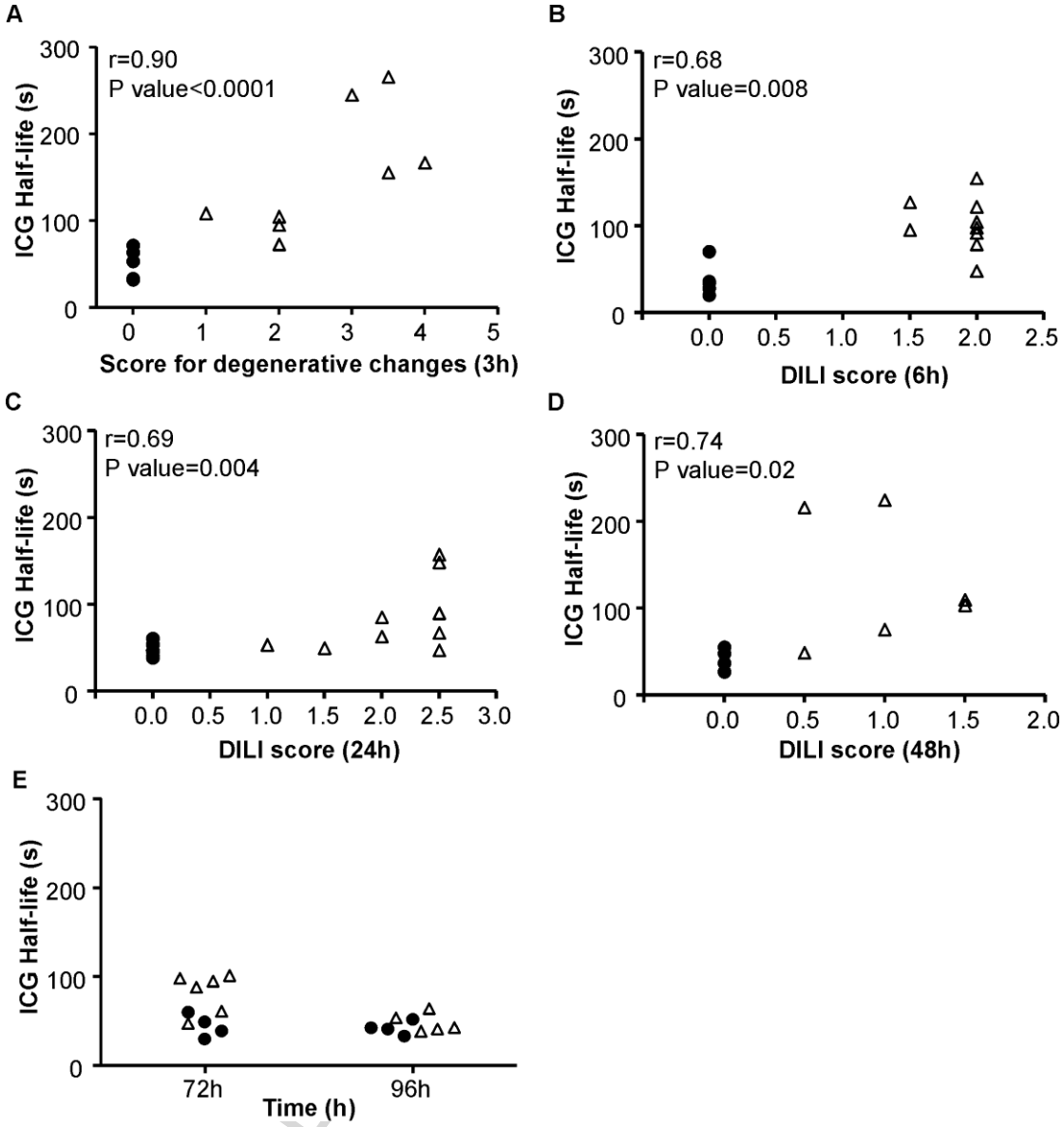

Figure 5

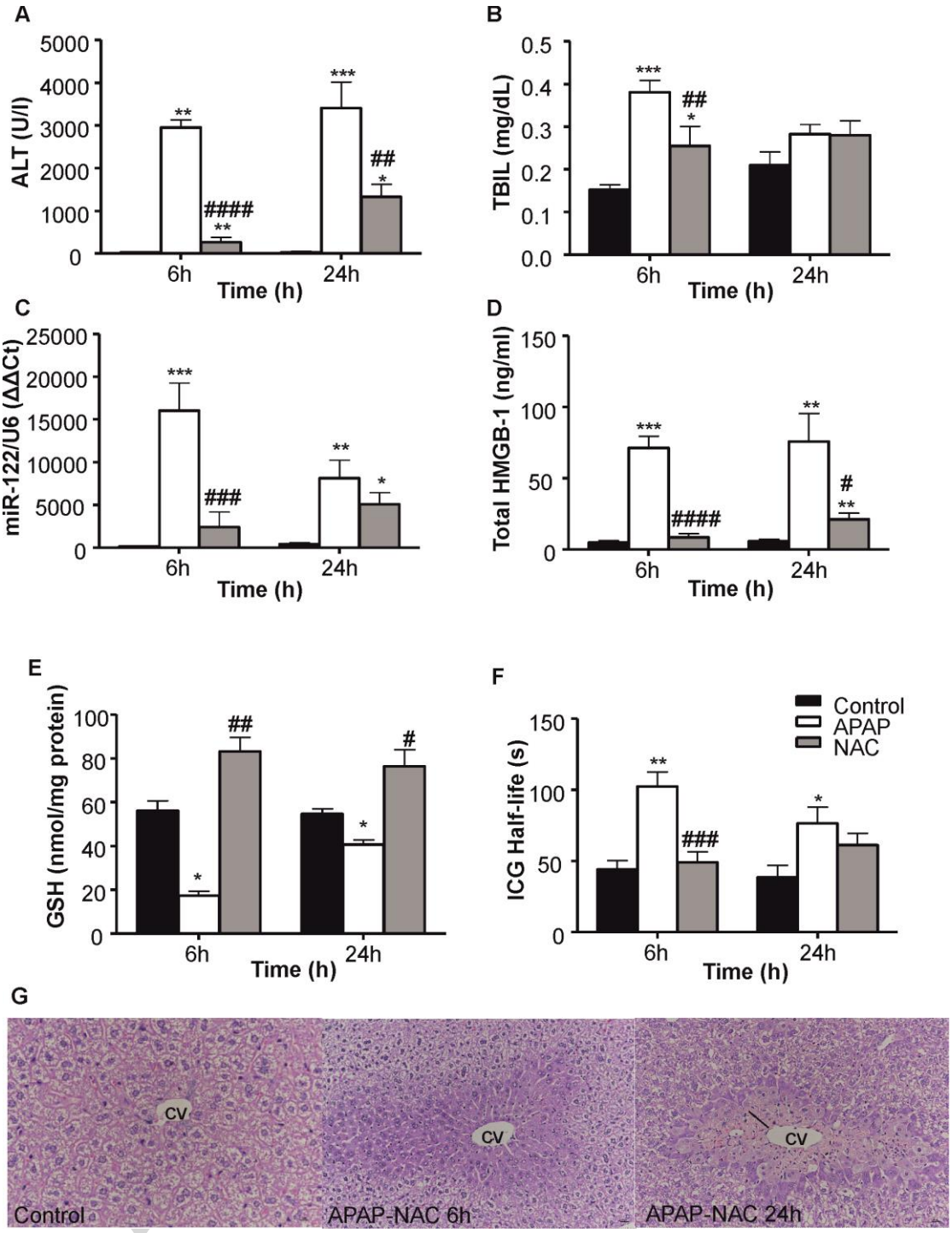

Figure 6

Conflict of interest statement

Conflict of Interest

All of the authors have no conflict of interest to report. Authors D Antoine and BK Park are inventors on a granted patent that is owned by the University of Liverpool and not licenced to anybody ('Detection and biomarkers of drug induced toxicity' US8748109 B2 (June 2014), European patient number: EP2449378 (March 2015), Japanese patient number: 5721707 (April 2015).

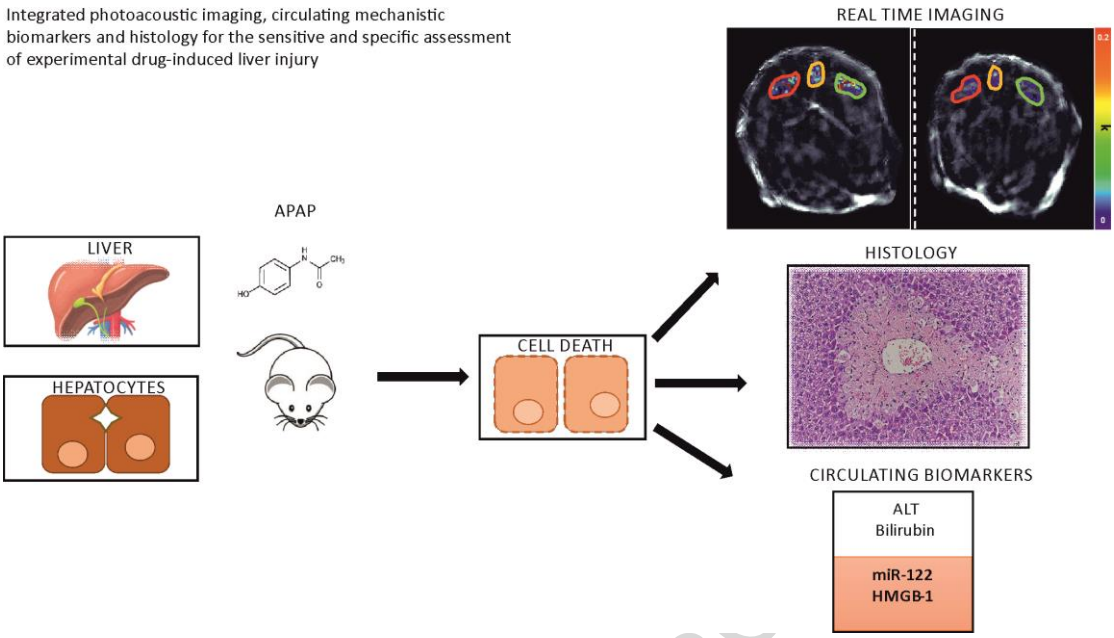

Graphical abstract

HIGHLIGHTS

- Imaging and circulating biomarker “tool box” proposed for liver injury and repair
- Liver function monitored in real time during acetaminophen hepatotoxicity
- Approach based on ICG clearance measured by MSOT
- ICG kinetics correlates with established methods for liver injury detection
- Approach can be used for prediction of response to therapeutic interventions